International Journal of Heat and Fluid Flow 106 (2024) 109287

Contents lists available at ScienceDirect

International Journal of Heat and Fluid Flow

journal homepage: www.elsevier.com/locate/ijhff

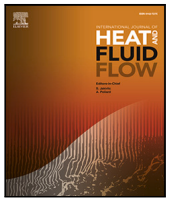

The role of the areal parameters on turbulent flow over 2D Gaussian roughness

F. Bruno [a], M. De Marchis [b,*], E. Napoli [b]

[a] Facoltà di Ingegneria e Architettura, Università degli Studi di Enna Kore, Italy
[b] Dipartimento di Ingegneria, Università degli Studi di Palermo, Italy

ARTICLE INFO

Keywords:
Roughness
LES
Effective slope
Turbulence

ABSTRACT

In the past decades, numerous efforts have been dedicated to establishing a direct correlation between a geometric parameter that represents wall roughness and the corresponding velocity reduction, known as the Roughness Function ΔU^+. This reduction is influenced by various statistical measures of roughness height, including average roughness height, peak-to-valley roughness distance, roughness root mean square, and Effective Slope, among others. It has been demonstrated that a singular measure of roughness height cannot sufficiently predict the Roughness Function across all turbulent regimes. Consequently, many studies have concentrated on identifying a universal correlation between roughness geometry and the downward shift of the mean velocity profile. In this study, we investigated the correlation between various geometrical parameters and the Roughness Function using Large Eddy Simulation (LES) techniques in channel flows at a friction Reynolds number of $Re_\tau = 400$. Given the complexity introduced by the random nature of irregular roughness, we explored specific aspects of the relationship between wall irregularities and the roughness function by studying 2D geometries. This approach allowed us to systematically investigate the impact of geometrical properties on the roughness function and isolate the effects of roughness density and coverage area. Several irregular rough surfaces, characterized by different average oscillations height, different distributions and different densities, were designed throughout 2D Gaussian functions. With the aim to find a universal correlation between the roughness geometry and the Roughness Function, new geometrical quantities were investigated, based on the global area occupied by the roughness A^*. The prediction of the roughness function can be thus obtained using apriori data. To predict the roughness function, we introduced a parameter called Effective Area (EA), which is derived from the correlation between the Effective Slope (ES) and the roughness area A^*. Our findings indicate that a single geometric parameter, whether ES or Area A, is insufficient to predict the roughness effect. Conversely, combining these two parameters enhances predictive accuracy, at least for the proposed roughness model. This improvement can be attributed to the ability of ES to interpret the roughness distribution and height, while the coverage area is effective in predicting roughness density over a flat plate.

1. Introduction

Which roughness length scales best typify a surface hydraulically? Since the early experimental works in the last decades, several researchers have been working to reply to this question. The attention of the scientific community on the roughness effect is clearly justified considering that, in almost all the engineering systems, the boundaries are characterized by irregularity and only seldom can be considered hydraulically smooth. Despite extensive efforts have been made to understand the turbulent flow physics over corrugated walls, through computational and laboratory experiments, the knowledge cannot be considered sufficiently robust and universal. This can be attributed to the large number of roughness topographies. In fact, surfaces become rough over time owing to deposition as well as time-related deterioration, including erosion, corrosion, organic and inorganic fouling processes. Basically, the roughness is somewhat of dynamic phenomena and it can induce dramatic reduction of the system performance and huge increase of the management costs. Hence, the prediction of the turbulence effects becomes an important prerequisite for optimal engineering design and machine maintenance.

Since the fundamental studies of Nikuradse (1993) and Moody (1944), the research of a geometric length scale able to predict the roughness effect on the mean flow was investigated. The preliminary

* Corresponding author.
E-mail address: mauro.demarchis@unikore.it (M. De Marchis).

https://doi.org/10.1016/j.ijheatfluidflow.2024.109287
Received 11 July 2023; Received in revised form 19 November 2023; Accepted 5 January 2024

experiments focused the attention on the relationship between wall frictional drag and sand grain roughness at different Reynolds number. One of the first contribution able to find a mathematical law to predict the main roughness effect was given by Hama (1954), introducing the correlation between a parameter, known as equivalent sand grain roughness k_s and the energy loss induced by the roughness. Hama (1954) focused the attention on the downward shift of the mean velocity profile in the log region, known as Roughness Function ΔU^+ (hereafter, the superscript $^+$ denotes variables made non-dimensional with inner variables $u_\tau = (\tau_s/\rho)^{0.5}$ and ν/u_τ, where u_τ is the friction velocity, τ_s is the wall stress, ρ the fluid density and ν the kinematic viscosity). This shift is correlated with the equivalent sand grain roughness k_s through the equation:

$$\Delta U^+ = \frac{1}{\kappa} ln(k_s^+) + B \tag{1}$$

where κ is the von Kàrmàn constant, $k_s^+ = k_s \cdot u_\tau/\nu$ and B is a constant. Unfortunately, k_s cannot be assigned a priori; it is not, in fact, a real geometric parameter and can be determined once the mean velocity profile in rough conditions is known. The prediction of the roughness-induced friction drag, merely based on the knowledge of the roughness topography, has received extensive attention in the past and a variety of roughness correlations have been developed in literature (see Sigal and Danberg (1990), Waigh and Kind (1998), Van Rij et al. (2002), Bons (2005), Napoli et al. (2008) and Flack and Schultz (2010)). More recently, experimental (Barros et al., 2018; Flack et al., 2020) and numerical (see among others Forooghi et al., 2017; Kuwata and Kawaguchi, 2019; Chan et al., 2015; Thakkar et al., 2017; Yang et al., 2022; Jouybari et al., 2021) studies have systematically analyzed rough surfaces to investigate on the effect 3D Gaussian and non-Gaussian geometries on the turbulent flows, focusing the attention on the roughness parametrization. Some widely discussed statistical measures in this context were summarized by Chung et al. (2021). The authors, in fact, investigated the average roughness height k^+, the peak-to-valley roughness distance k_{pv}^+, the roughness root mean square k_{rms}^+, the skewness S_k, the Effective Slope ES, the density parameter λ_s and the correlation length L_{corr}. The extensive works carried out in the past, as highlighted by Flack and Schultz (2014), showed how a single roughness feature, is not able to adequately predict the Roughness Function. Indeed, a single parameter can be representative of a single feature of the roughness: the height or the asymmetry or the randomness, etc. Therefore, a number of questions regarding the relationship between ΔU^+ and a physical measure of the surface irregularities, applicable in both the transitionally and fully rough regimes, are still open. This is mainly due to the heterogeneity of rough topography. In literature, in fact, wall roughness was reproduced with 2D or 3D elements or was distributed through regular or irregular shapes (see among others Napoli et al., 2008; Schultz and Flack, 2009). The earliest studies focused the attention on regular geometry and distribution, involving ribbed, cubed or spherical elements (see Leonardi et al. (2003), Antonia and Krogstad (2001), Ashrafian et al. (2004), Bhaganagar et al. (2004), Lee et al. (2022) and Orlandi et al. (2006)). One of this contribution was given by Schlichting (1937) who compared the effect of several different roughness elements (spheres, cones, hamburg sand, etc.) on the mean flow. The author highlighted the dependence of the wall resistance on both the roughness height and a parameter, defined as solidity, related to the element density and defined as $\lambda = \frac{A_P}{A_T}$, where A_P is the projected plan area of a roughness element, which occupies an area A_T on the wall. Following the definition of the solidity, Sigal and Danberg (1990) performed a number of studies to determine a suitable geometric correlation relating to the roughness density effect. Their new roughness density parameter, known as λ_s, reads $\lambda_s = \frac{S}{S_f} \cdot \left(\frac{A_f}{A_s}\right)^{-1/6}$, where S is the plan form area of the corresponding smooth surface, S_f is the total frontal area of all roughness elements (S and S_f are equivalent to those used in Schlichting's studies), A_f is the frontal area of a single roughness element and A_s is the wetted area of a single roughness element. Within this correlation, (S/S_f) represented a roughness density parameter and (A_f/A_s) represented a roughness shape parameter. More recently, Napoli et al. (2008), introduced the Effective Slope ES, similar to the solidity and defined as $ES = \frac{1}{L_{x_1}} \int_{L_{x_1}} \left|\frac{dk(x_1)}{dx_1}\right| dx_1$, where $k(x_1)$ is the roughness height along the streamwise direction and L_{X_1} is the respective streamwise lengths of the rough surface. Extensive investigations on the effects of solidity and of the Effective Slope were also conducted by Leonardi and Castro (2010), as well as Macdonald et al. (2016), who pointed out that ES is strictly connected with the concept of the solidity, $ES = 2 \cdot \lambda$. Subsequent researches, carried over 2D and 3D roughness elements, both regularly or irregularly distributed (see among others Yuan and Piomelli, 2014; Anderson et al., 2015; Busse et al., 2015; De Marchis, 2016; Milici and De Marchis, 2016), observed a direct correlation between the downward shift of the mean velocity profile ΔU^+ and ES. The dependence of the ΔU^+ on ES was studied by Schultz and Flack (2009) in their analysis on close-packed pyramids characterized by different value of height and slope. The achieved results were then confirmed by Chan et al. (2015) through Direct Numerical Simulations (DNSs) over sinusoidal wavy walls and by Forooghi et al. (2017) over randomly distributed semi-ellipsoid/cone roughness and more recently by Garg et al. (2023). Despite the overall effectiveness of the correlation between ES and turbulent flows, some independent studies have observed that roughness with different geometries but the same ES can result in varying values of the Roughness Function (Schultz and Flack, 2009; Mejia-Alvarez and Christensen, 2013; Macdonald et al., 2016; De Marchis et al., 2020). This observation underscores the necessity for further investigation into this specific parameter. Many other geometrical statistical quantities have been investigated in order to find a direct correlation between roughness type and effects on turbulent flows. Some authors focused the attention on the skewness factor of the roughness oscillations (Flack and Schultz, 2010; Chan et al., 2015; Thakkar et al., 2017). Flack and Schultz (2010), thanks to a large amount of experimental data for different types of rough surfaces, proposed a new correlation between S_k and k_s. The authors continued to investigate this aspect revealing that a dramatic increase in friction drag occurred when the S_k value changed from a negative value to zero, while a change from zero to a positive value caused a modest increase in friction drag (Flack et al., 2020). Nevertheless, Busse et al. (2017) and Flack et al. (2020) showed how some turbulent features are almost independent of the skewness factor.

Looking at the researches performed over irregular rough walls, some studies specifically focused their efforts on the correlation between ΔU^+ and the roughness geometry. Among the more recent investigations, Thakkar et al. (2017) applied DNS techniques to study the effect of roughness topography on 17 industrially relevant irregular surfaces. The authors proposed a correlation between ΔU^+ and λ, S_k, and k_{rms}. Jouybari et al. (2021) developed a high-fidelity prediction approach of k_s for turbulent flows over 45 different surface geometries. To this end, Deep Neural Network (DNN) and Gaussian Process Regression (GPR) machine learning approach was used to find a mapping of 17 different rough surface statistics to equivalent sand-grain height. The surface parameters include 8 primary variables widely investigated in literature (k, k_{rms}, R_a, ES_x, ES_z, Sk, Ku, nc_{xi}) and 9 products of them such as $ES_x{*}k$, $Sk{*}Ku$ and so on. The authors pointed out that there is some correlation between kurtosis and rms roughness and kurtosis and skewness, conversely the relationship between others parameters appears to be more random. A formulation to predict k_s was recently proposed by Abdelaziz et al. (2022). The authors performed laboratory experiments in a zero pressure gradient turbulent boundary layer, to investigate the downward shift of the mean velocity profile, in the streamwise direction, induced by two-dimensional rough surfaces. While k_s is not an actual physical roughness parameter that can be measured directly from the topology of the surface, the authors proposed a new expression for k_s involving some physical roughness

parameters. The study shows that the equivalent sand grain roughness can be correlated with the mean roughness height, the effective slope ES and the skewness S_k. The authors pointed out the importance to analyze simple 2D uniformly distributed roughness shapes and confirmed how a relation proposed for 2D rough wall can be applied also for 3D rough geometries. They concluded that a general scaling cannot exist because of the complexity of the roughness geometries which involve too the many parameters. Similar considerations have been discussed by Chung et al. (2021) who observed that there is not a universal model able to accurately predict the drag from a sufficiently wide range of roughness. This is mainly attributed to the high-dimensional feature space of irregular rough structures. The effects of several geometrical parameters on the Roughness Function was investigated by De Marchis et al. (2020), through Large Eddy Simulation (LES) on irregularly roughened textures obtained by the superimposition of four sinusoidal functions of different wavelengths and random amplitudes. The authors analyzed the effect of more than a single geometrical parameter and they reported a correlation between the ES and the root mean square of the wall oscillation k^+_{rms}, as well as between ES and the mean absolute deviation $\overline{k}^+$. Specifically, the authors observed that a single geometrical feature of the roughness cannot be able to estimate the roughness function. In fact, a lot of data having the same ES or k^+ or k^+_{rms} values, are characterized by very different ΔU^+. On the other hands, they reported a specific trend analyzing data in term of $ES \cdot k^+$ and $ES \cdot k^+_{rms}$. The authors also tried to correlate k^+ with other geometrical parameters without finding a specific correlation. The paper suggested that a combination between the Effective Slope with a geometrical parameter may be the key to predict the Roughness Function. The results obtained by De Marchis et al. (2020) has been confirmed by the independent study of Zhen Ma et al. (2022), where a good correlation between ΔU^+ and $\overline{k}^+ \cdot ES$ was found. The above analysis clearly pointed out the importance to find a geometrical feature of the roughness able to be representative of the effect on turbulent flows. Furthermore, it is evident that a combination between two or more roughness length scales can better represent the roughness geometry.

In order to contribute on this fundamental issue, a systematic study of 2D irregular rough surfaces, having different height and density, is performed. Furthermore, the attention is focused on the impact of roughness density and coverage roughness area on the mean flow. Similar analyses have been recently carried out by Nugroho et al. (2023) and Sarakinos and Busse (2022) confirming the significance of coverage area in understanding roughness effects. Specifically, Sarakinos and Busse (2022) examined idealized barnacle-shaped roughness, considering a range of roughness coverage from 10% to 85%. Their findings revealed that the ΔU^+ peaked at 60% coverage. On the other hand, Nugroho et al. (2023) investigated the relationship between skin friction drag and the coverage area of surface roughness. Their results demonstrated an increase in the Hama roughness function as roughness area coverage increased from 5% to 30%. Unfortunately, these studies did not investigate the correlation between ΔU^+ and a specific areal parameter. Our study is dedicated to addressing this gap by attempting to establish such a correlation. Given the complexity introduced by the random nature of irregular solid walls, 2D roughness elements have been studied to isolate the effects of roughness density and height, thus to isolate the effects of the roughness area amount. Resolved LES have been performed over irregularly roughened surfaces having different roughness distribution and shapes.

The organization of the paper is as follow: Section 2 describes the numerical code adopted for LES, Section 3 highlights flow conditions and numerical parameters, whereas the roughness parameters are described in Section 4; results are presented in Section 5 and conclusions are drawn in Section 6.

2. Mathematical model and numerical procedure

The turbulent channel flow is resolved using the LES technique, based on the numerical solution of the filtered Navier–Stokes and continuity equations for incompressible fluids given by:

$$\frac{\partial \overline{u}_i}{\partial t} + \frac{\partial \overline{u}_i \overline{u}_j}{\partial x_j} - \frac{1}{Re_\tau}\frac{\partial^2 \overline{u}_i}{\partial x_j \partial x_j} + \frac{\partial \overline{p}}{\partial x_i} + \frac{\partial \tau_{ij}}{\partial x_j} + \Pi\ \delta_{i1} = 0 \tag{2}$$

$$\frac{\partial \overline{u}_i}{\partial x_i} = 0 \tag{3}$$

the symbol $\bar{\cdot}$ is applied for filtered quantities. All the terms reported in Eqs. (2) and (3) are non-dimensional. In particular, the velocities $\overline{u}_i$ are normalized with the friction velocity u_τ and the spatial coordinates x_i with the channel half height h, t is time normalized with u_τ/h, $\overline{p}$ is the kinematic pressure field (pressure divided by density and u_τ^2), δ_{i1} is the Kronecker function and $Re_\tau = u_\tau h/\nu$ is the friction Reynolds number. The last term Π is the non-dimensional imposed pressure gradient driving the flow. Hereafter x_1 indicates the streamwise direction, x_2 indicates the spanwise direction and x_3 indicates the wall-normal direction. In statistically steady-state conditions, the equilibrium between the imposed driving stress and the overall streamwise component of the wall stress holds, thus:

$$\Pi_d = \frac{\tau^{up}_{s,d} + \tau^{down}_{s,d}}{2h} = \frac{\tau_{s,d}}{h} \tag{4}$$

where the average wall stress reads $\tau_{s,d} = \frac{1}{2A}\int_A \left[\mu \frac{\partial u_{s,d}}{\partial n}\mathbf{t}\cdot\mathbf{s} - p_d \mathbf{n}\cdot\mathbf{s}\right] dA$. A is wall wet surface, u_s is the tangential velocity component, $\mathbf{t}$ and $\mathbf{n}$ are the tangential and normal unit vectors to the wall surface element dA. Finally, $\mathbf{s}$ is the streamwise direction vector. Since the equations are made non-dimensional with the friction velocity $u_\tau = \sqrt{\tau_{s,d}/\rho}$ and the half-channel height h, it is always $|\Pi_d| = 1$. The momentum and continuity equations are resolved using the finite-volume numerical code PANORMUS (PArallel Numerical Open-souRce Model for Unsteady flow Simulations) which is second-order accurate both in time and space (Napoli et al., 2008). The numerical model uses the explicit Adams–Bashforth method for the time advancement of the solution, while the fractional-step technique is used to overcome the pressure–velocity decoupling, in conjunction with the multigrid accelerator V-cycle. The Sub-Grid Scale turbulent stress tensor τ_{ij} is modeled using the Dynamic Mixed Model (DMM) of Zang et al. (1993). The quality of the numerical code in simulating turbulent channel flows has been extensively validated over smooth as well as rough conditions. Specifically, the results over smooth walls were compared with the available data of Moser et al. (1999), whereas the results obtained simulating wavy wall roughness were compared with the DNS data published by Maaß and Schumann (1996). In both cases a very satisfying agreement with the reference data was achieved. Details on the numerical procedure and on the sub-grid model can be found in De Marchis et al. (2019, 2020). The numerical model was furthermore extensively and favorably validated over a wide range of cases (Napoli et al., 2008; De Marchis et al., 2010; De Marchis and Napoli, 2012; De Marchis, 2016; De Marchis et al., 2020). A discussion on the performed validation tests up to $Re_\tau = 1000$, in turbulent channel flows, is reported in De Marchis et al. (2020).

3. Physical and numerical parameters

The wall roughness is investigated reproducing irregular geometries in an archetypal way. Specifically, 2D rough surfaces were designed throughout Gaussian distribution. Thanks to the Gaussian function is possible to modulate the roughness geometry modifying the standard deviation and generate rough shapes having different geometrical parameters. In the proposed study, several numerical simulations were performed considering irregular roughness having different average oscillation, different distribution and different density. Specifically, turbulent channel flows were investigated at five increasing roughness

average height equal to $\overline{k} = 0.005 \cdot h$, $\overline{k} = 0.01 \cdot h$, $\overline{k} = 0.02 \cdot h$, $\overline{k} = 0.03 \cdot h$, $\overline{k} = 0.04 \cdot h$. For each value of roughness height, different roughness densities were considered through the imposition of 32 or 64 subsequent positive and negative Gaussian functions. Indeed, as shown in the following, 64 Gaussian functions generate highest roughness densities. Both upper and lower walls were generated using the following equation:

$$k[x_1(ii)] = \sum_{i=1}^{32 \cdot jj} \beta \sum_{j=1}^{8/jj} \frac{1}{\sigma_i \sqrt{2\pi}} e^{-\frac{1}{2}\left(\frac{x_1(j)-\mu}{\sigma_i}\right)^2} \tag{5}$$

where the parameter μ is the mean of the distribution (and also its median and mode), whereas σ is the standard deviation. Specifically, the standard deviation σ_i is randomly generated in a range between $B < \sigma_i < 1 + B$, with B a constant of the specific geometry. β is equal to +1 when i is even, whereas $\beta = -1$ for odd value of i. Moreover, $ii = i \cdot j$ and $jj = 1$ for the cases having 32 subsequent Gaussian functions, whereas $jj = 2$ for 64 Gaussian. The parameter μ is kept constant equal to $\frac{4\pi}{16}$. Due to the randomness of σ, upper and lower walls have different shape even though their share the statistics. Fig. 1 shows the 3D sketch of the computational domain for two surfaces, having 32 and 64 Gaussian functions. The domain is sized $4\pi h \times \pi h \times 2h$ in the x_1, x_2 and x_3 direction, respectively and it has been discretized using $256 \times 64 \times 64$ computational cells, along x_1, x_2 and x_3 directions. Thanks to the periodic condition a uniform distribution has been applied in the x_1 and x_2 direction, resulting in $\Delta x_1^+ = 19.6$ and $\Delta x_2^+ = 19.6$. On the other hand a non-uniform mesh has been used in the x_3 direction. Specifically, in wall-normal direction the points are clustered near the wall ensuring a minimum cell size equal to $\Delta x_{3min}^+ = 0.5$. The mesh increase toward the channel centerline thus to have $\Delta x_{3max}^+ = 26.5$. To simulate the turbulent channel flow, periodic boundary conditions are imposed in both the streamwise and spanwise directions., while the no-slip condition is enforced at the rough walls. Curvilinear structured boundary-fitted grids are used to discretize the computational domain. All simulation were carried out at friction Reynolds number equal to $Re_\tau = 400$. The numerical simulations have been performed at relatively low Reynolds number, especially compared with some recent DNS and LES studies over rough surfaces, where friction Reynolds numbers up to 1000 have been investigated (see Forooghi et al. (2017) and De Marchis et al. (2020)). Despite of this in rough wall cases, the correlation obtained for $Re_\tau = 400$ between geometric parameters and roughness functions is valid also for Reynolds values higher than $Re_\tau = 1000$ (De Marchis et al., 2020), ensuring the generalization of the achieved results.

4. Roughness parameters

One of the main challenge in the study of turbulent flow over rough surfaces is to find a geometrical parameter able to match the stochastic nature of random roughness and its effect on the flow. Therefore, following recent researches (see among others De Marchis et al., 2020; Anderson et al., 2015; Jouybari et al., 2021; Zhen Ma et al., 2022; Ganju et al., 2022), in the proposed study, several surface parameters were analyzed for a number of roughness shapes. In Table 1 the definition and the values of the most widely used roughness parameters are reported, whereas in Table 2, details on the studied geometrical quantities are reported. Using a height-map to characterize the surface from the zero plane (Chung et al., 2021), some of geometrical data are represented in Fig. 2.

Among the most studied parameter, those based on the roughness density (see Sigal and Danberg (1990)) or ES (Napoli et al., 2008), seem to have a very good correlation with the flow resistance. The roughness area, less analyzed in literature, take into account of the roughness density. In order to investigate on this issue, geometrical parameters able to reflect the roughness area, were introduced. Specifically, four roughness areal parameters, based on the filled part of the Gaussian rough profile, plotted in Fig. 3, were defined. Fig. 3a shows

Table 1
Definition of roughness parameters.

$\overline{k}$	Average roughness height	$\frac{1}{n}\sum_{i=1}^{n} \lvert x_{3,i} \rvert$
k_{max}	Maximum peak to valley above the zero plane	$max(x_3)$
k_{min}	Maximum valley depth below the zero plane	$min(x_3)$
k_{pv}	Maximum peak to valley height of the profile	$k_{max} + \lvert k_{min} \rvert$
k_{rms}	Root mean square roughness height	$\sqrt{\frac{1}{n}\sum_{i=1}^{n} {x_{3,i}}^2}$
S_k	Skewness	$\frac{1}{n(k_{rms})^3}\sum_{i=1}^{n} x_{3,i}^3$
K_u	Kurtosis	$\frac{1}{n(k_{rms})^3}\sum_{i=1}^{n} x_{3,i}^4$
ES	Effective slope	$\frac{1}{L_{x_1}}\int_{L_{x_1}} \left\lvert \frac{\partial k(x_1)}{\partial x_1} \right\rvert dx_1$

the peaks area above the zero plane, indicated as A_P; Fig. 3b shows the peaks area above the absolute average deviation $\overline{k}$, indicated with $A_{P\overline{k}}$; Fig. 3c plots the area of the absolute value of Gaussian peaks and cavities $\overline{A}$. Finally, Fig. 3d shows the area of the absolute value of Gaussian peaks and cavities above the absolute average deviation $\overline{k}$, indicated with $\overline{A}_{\overline{k}}$.

The above normalized areal parameters are calculated according to the following equations:

$$A_P = \int_0^{L_{x_1}} f(x_3) dx_1 \qquad \text{for} \qquad x_{3,i} > 0 \tag{6}$$

$$A_{P\overline{k}} = \int_0^{L_{x_1}} \left(f(x_3) - \overline{k} \right) dx_1 \qquad \text{for} \qquad x_{3,i} > 0 \tag{7}$$

$$\overline{A} = \int_0^{L_{x_1}} |f(x_3)| dx_1 \tag{8}$$

$$\overline{A}_{\overline{k}} = \int_0^{L_{x_1}} \left(|f(x_3)| - \overline{k} \right) dx_1 \tag{9}$$

where $f(x_3)$ is the function obtained through Eq. (5). In Table 3 the above areal parameters are reported.

5. Results

5.1. Mean velocity profiles

The mean streamwise velocity profile is one of the main indicator of the effect of wall roughness on turbulent flows. Indeed, wall asperities are responsible of the downward shift of the mean velocity profiles. Compared to the smooth wall case, as previously mentioned, the distance between smooth and rough velocities in the logarithmic region, represents the Roughness Function ΔU^+. Therefore, the following results focus the attention on the effect of corrugated walls on the velocity reduction. Hereafter, the shown statistical quantities are made non-dimensional with the friction velocity u_τ; moreover with the symbol $\langle \cdot \rangle$ the data averaged in time, over the statistical homogeneity planes $x_1 - x_2$ and taking advantage of symmetry with respect to mid-plane, are indicated. In the following figures, the non-dimensional wall distance x_3^+ is measured from the flat reference plane to which the Gaussian functions are superimposed to generate the wall roughness. Usually x_3^+ should be measured from the plane at which the total drag acts, frequently referred as "zero-plane displacement". Following several authors the zero-plane displacement was obtained by optimizing the fit of the spatially averaged mean velocity to the log-linear profile. The results confirmed the identification of the origin in $x_3^+ = 0$.

Fig. 4a–b show the mean velocity profiles in the streamwise direction achieved for all the numerical simulations performed at $Re_\tau = 400$. In Fig. 4a, the results of the simulations characterized by the subsequent 32 Gaussian shapes, are plotted (see the geometry sketch depicted in Fig. 1a). As expected, the picture clearly shows an increase of the downward shift of the velocity, increasing the mean roughness height from $\overline{k} = 0.005 \cdot h$ to $\overline{k} = 0.04 \cdot h$ (see Table 3). Fig. 4b shows the mean velocity profiles achieved over irregular roughness surfaces characterized by a density of 64 Gaussian shapes (see the 3D representation of

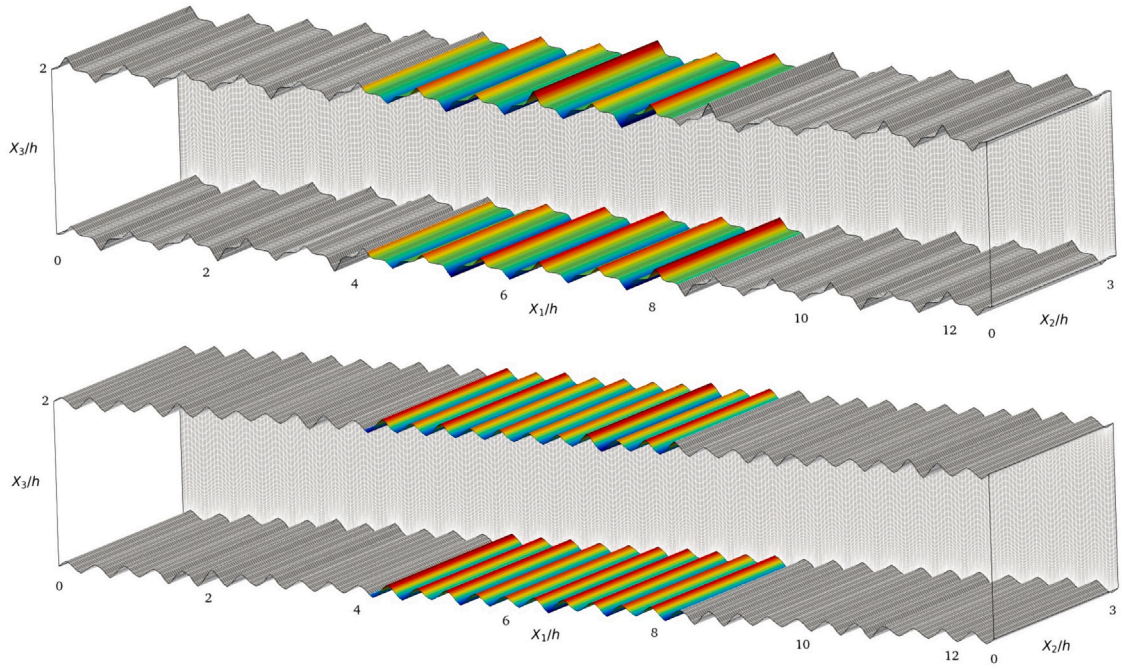

Fig. 1. 3D sketches of irregular rough channel. Top panel: 32 Gaussian functions configuration; Bottom panel: 64 Gaussian functions configuration.

Table 2
Geometrical and flow properties for the Gaussian roughness. $\bar{k}/h$: average roughness height. $\overline{k^+}$: mean roughness height. k^+_{max}: maximum roughness height. k^+_{pv}: maximum peak to valley height of the profile. k^+_{rms}: root mean squares of the wall roughness. ES: Effective Slope. S_k: skewness. K_u: kurtosis.

Marker	*Sketch*	*Case*	*NG*	$\bar{k}^+$	k^+_{max}	k^+_{pv}	k^+_{rms}	*ES*	S_k	K_u
–		Flat	0	0.0	0.0	0.00	0.00	0.00	0.00	0.00
●		I32_0.5	32	2.00	7.38	14.74	5.99	0.08	0.06	3.36
●		I32_1	32	3.98	16.49	32.55	6.08	0.16	0.17	3.62
●		I32_2	32	7.98	33.08	69.22	12.20	0.33	-0.24	3.67
●		I32_3	32	11.98	56.47	112.27	18.56	0.49	0.18	4.05
●		I32_4	32	15.98	83.30	135.74	24.61	0.65	-0.08	3.89
♦		I64_0.5	64	2.00	4.18	8.40	2.37	0.09	0.04	1.86
♦		I64_1	64	3.98	9.24	18.66	4.81	0.18	0.04	1.86
♦		I64_2	64	7.98	19.68	38.09	9.68	0.37	-0.10	1.92
♦		I64_3	64	11.98	27.80	56.17	14.48	0.55	0.06	1.87
♦		I64_4	64	15.98	43.00	87.81	19.57	0.74	0.10	2.09

the rough domain plotted in Fig. 1b). The profiles confirm that the more the roughness height the more the Roughness Function. This behavior can be attributed to the augmentation of energy dissipation induced by wall oscillations. Interestingly, all the profiles share the same slope regardless the roughness conditions and it is equal to the classical von Kàrmàn constant suggesting the validity of the log region.

Table 3
Details on the roughness type and the related areal parameters, normalized with outer length scale. A_P^+: Peaks area above the zero plane. $A_{P\overline{k}}^+$: Peaks area above the absolute average deviation. $\overline{A}^+$: Area of the absolute value of Gaussian peaks and cavities. $\overline{A}_{\overline{k}}^+$: Area of the absolute value of Gaussian peaks and cavities above the absolute average deviation.

Marker	Sketch	Case	NG	A_P^+	$A_{P\overline{k}}^+$	$\overline{A}^+$	$\overline{A}_{\overline{k}}^+$
●		I32_0.5	32	9.96E+03	2.60E+03	1.51E+04	5.09E+03
●		I32_1	32	2.54E+04	5.38E+03	3.02E+04	1.02E+04
●		I32_2	32	4.97E+04	9.54E+03	6.06E+04	2.05E+04
●		I32_3	32	7.64E+04	1.62E+04	9.10E+04	3.08E+04
●		I32_4	32	1.00E+05	1.98E+04	1.21E+05	4.11E+04
♦		I64_0.5	64	1.13E+04	1.35E+03	1.25E+04	2.56E+03
♦		I64_1	64	2.28E+04	2.77E+03	2.54E+04	5.38E+03
♦		I64_2	64	4.57E+04	5.57E+03	5.12E+04	1.11E+04
♦		I64_3	64	6.88E+04	8.61E+03	7.65E+04	1.63E+04
♦		I64_4	64	9.08E+04	1.05E+04	9.08E+04	2.25E+04

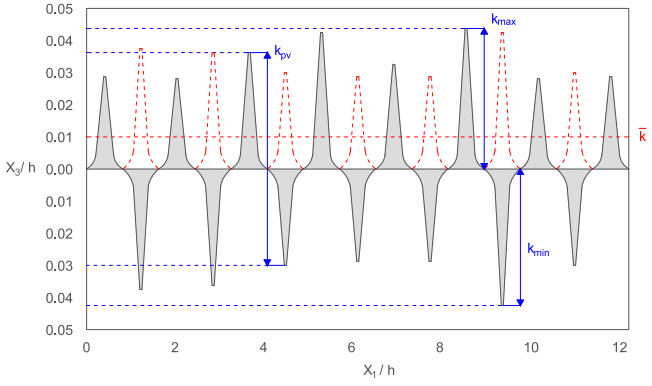

Fig. 2. Schematic representation of geometrical data. $\overline{k}$: average roughness height. k_{pv}: maximum peak to valley height of the profile. k_{max}: maximum peak to valley above the zero plane. k_{min}: maximum valley depth below the zero plane.

In order to verify this validity and to calculate the effective value of the Roughness Function, in Fig. 4c–d, the difference in the mean velocity profile between the smooth and rough cases ($\delta U^+ = \langle U_F^+ \rangle - \langle U_R^+ \rangle$) is depicted. The profiles remain fairly constant in the region above $x_3^+ = 100$, confirming the qualitative findings observed in Fig. 4a–b, where all the distributions share the slope of the mean velocity profiles. Therefore, the ΔU^+ has been obtained averaging the δU^+ value in the log-region.

In Table 4 the flow properties of the simulations over rough surfaces are reported. Specifically, the friction Reynolds number, the centerline Reynolds number, the bulk Reynolds number, the normalized centerline mean velocity and the bulk velocity were calculated. In addition, the Table summarizes the values of Roughness Function and equivalent sand-grain roughness which can be estimated after the mean velocity

Table 4
Flow properties of the numerical simulations. Re_τ, Re_{cl} and Re_b are the friction, centerline and bulk Reynolds number. U_{cl^+} is the normalized centerline mean velocity, U_{b^+} is the normalized bulk velocity. The ΔU^+ is the Hama Roughness Function and k_s^+ is the equivalent sand grain roughness.

Marker	Case	NG	Re_τ	Re_{cl}	Re_b	U_{cl^+}	U_{b^+}	U_{cl^+}/U_{b^+}	ΔU^+	k_s^+
●	I32_0.5	32	400	7443	6427	18.61	16.07	1.16	1.65	12.80
●	I32_1	32	400	5980	5030	14.95	12.57	1.19	5.12	26.00
●	I32_	32	400	3960	3095	9.90	7.74	1.28	9.91	188.00
●	I32_3	32	400	3000	2129	7.50	5.32	1.41	12.55	520.00
●	I32_4	32	400	2504	1686	6.26	4.21	1.49	13.31	840.00
♦	I64_0.5	64	400	7588	6553	18.97	16.38	1.16	1.41	12.00
♦	I64_1	64	400	6181	5175	15.45	12.94	1.19	4.87	24.00
♦	I64_2	64	400	4760	3824	11.90	9.56	1.24	8.33	100.00
♦	I64_3	64	400	3971	3067	9.93	7.67	1.29	10.17	180.00
♦	I64_4	64	400	3391	2517	8.48	6.29	1.35	11.24	360.00

profile is known. In fact, k_s^+ can be calculated equating, in the log region, the mean streamwise velocity profile with the wall law for the mean velocity in a rough-wall turbulent boundary layer. According to Ligrani and Moffat (1986), in the transitional regime the equivalent sand grain roughness has been estimated through the equation:

$$U^+ = \frac{1}{\kappa} ln(x_3^+) + C_s + (8.5 - Cs - \frac{1}{\kappa} ln(Re_{k_s})) \cdot sen(\frac{\pi \cdot G}{2}) \tag{10}$$

where

$$G = \frac{ln(\frac{Re_{k_s}}{5})}{ln(\frac{70}{5})}; \quad Re_{k_s} = \frac{k_s \cdot u^*}{\nu} \tag{11}$$

When the fully rough regime is achieved, the following equation is applied:

$$\frac{1}{\kappa} ln(x_3^+) + C_s - \Delta U^+ = \frac{1}{\kappa} ln(x_3^+ / k_s^+) + 8.5 \tag{12}$$

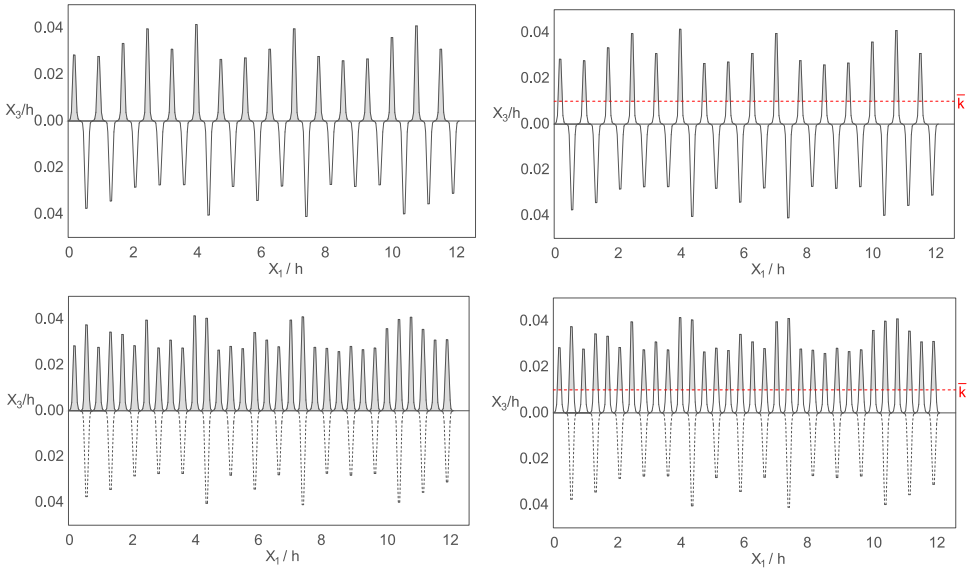

Fig. 3. Areal parameters estimation, based on the rough profile. (a) Peaks area above the zero plane: A_P. (b) Peaks area above the absolute average deviation $\overline{k}$: $A_{P\overline{k}}$. (c) Area of the absolute value of Gaussian peaks and cavities: $\overline{A}$. (d) Area of the absolute value of Gaussian peaks and cavities above the absolute average deviation $\overline{k}$: $\overline{A}_{\overline{k}}$.

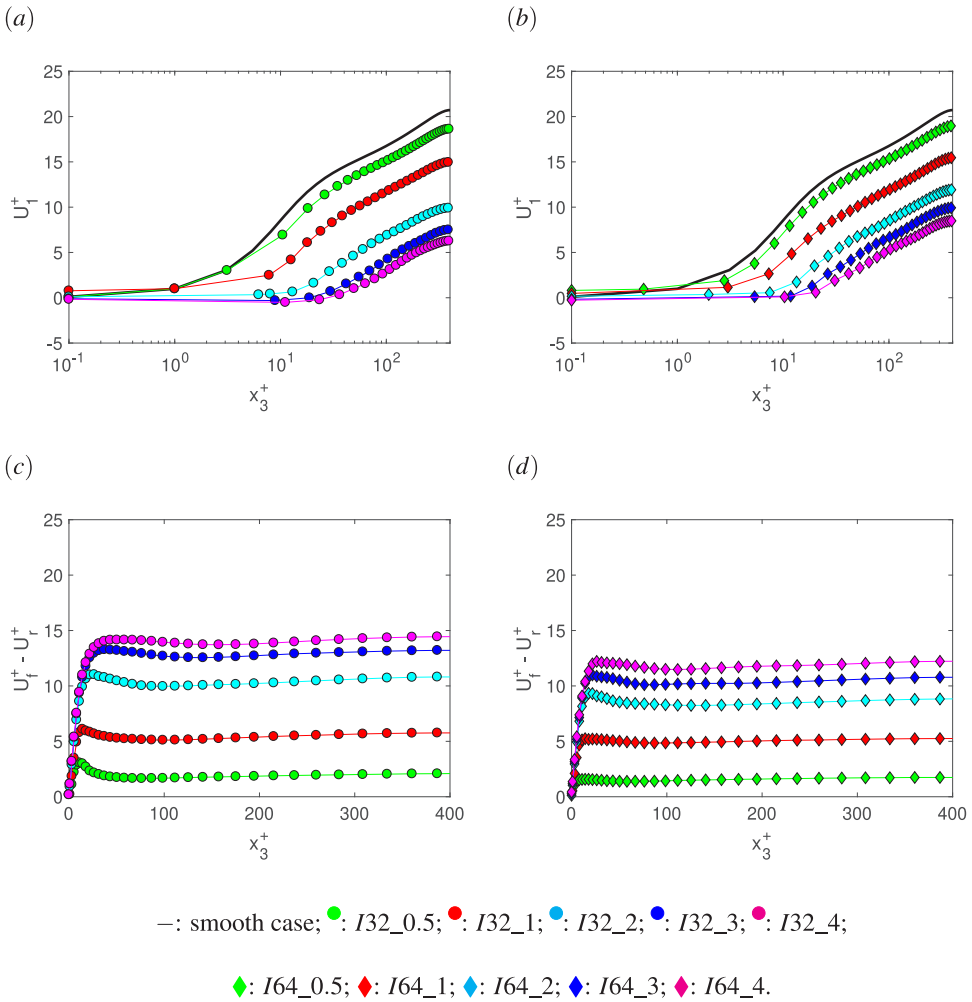

Fig. 4. (a) Mean streamwise velocity profile for the smooth wall and cases I32. (b) Mean streamwise velocity profile for the smooth wall and cases I64. (c) Difference in the mean velocity profile between the smooth and rough cases I32. (d) Difference in the mean velocity profile between the smooth and rough cases I64.

In Eqs. (10), (11) and (12) the mean velocity, as well as the roughness function, is obtained by the numerical mean velocity profile, whereas C_s is the classical additive constant for smooth case.

Several authors have performed numerical and experimental analyses to investigate the dependence of the roughness type on the different flow regimes. As pointed out by Flack and Schultz (2014), when $\overline{k}^+$ is small, the perturbations generated by the roughness elements are damped out by the fluid viscosity. For this condition, the flow is hydraulically smooth and $\Delta U^+ = 0$. This regime is conventionally observed for $k_s < 5$. Increasing $\overline{k}^+$, viscosity no longer damps out the eddies and the roughness elements start to increase the pressure drag, with a substantial balance between friction and pressure resistance. This is the transitionally rough regime, achieved for $5 < k_s^+ < 70$. A further increases of the roughness height causes the migration toward fully rough regime ($k_s^+ > 70$), where the skin friction is independent of Reynolds number and form drag, on the roughness elements, is the dominant mechanism. In the present research, 4 numerical simulations have an equivalent sand grain roughness in the range $5 < k_s^+ < 70$, thus to drop into transitional regime, whereas 6 simulations fall in the fully rough regime.

The velocity reduction in the streamwise direction is certainly guided by the roughness shape. The rough geometry can be correctly interpreted only through a combination of geometrical parameters, while a single feature of the corrugation geometry may not be representative of the whole effect. In this framework, to predict the Roughness Function or the equivalent sand grain roughness a parameter combination could be considered. This issue was recently highlighted by Jouybari et al. (2021). The authors provided a database to predict the equivalent sand-grain height for several rough geometries, also applying modern technique of Machine Learning to take into account for several parameters. In the following, the possible correlation between the mean flow fields and geometrical parameters is investigated.

5.2. Roughness function correlation

One of the main challenge correlated with the effect of the roughness on turbulent flow is the prediction of the mean velocity reduction, in the core region (i.e. the Roughness Function ΔU^+), once the geometry is a-priori known. Nowadays, rough walls can be precisely characterized through surface scan, indeed, roughness parameters can be easily determined. In this framework, the ability to determine the correlation between ΔU^+ and a geometric feature k^* is a key issue in the turbulence analysis. In Fig. 5 the correlations with the geometrical data reported in Table 2 are plotted. Specifically, the average roughness height $\overline{k^+}$, the maximum roughness peak height k^+_{max}, the root-mean square roughness height k^+_{rms}, the maximum roughness peak-to-valley height k^+_{pv}, the Effective Slope ES and the equivalent sand grain k_s^+ are analyzed. In the Figure, literature data of De Marchis et al. (2010) and De Marchis (2016) are included too. The picture clearly illustrates how a single parameter is not able to correctly predict the ΔU^+. In fact, geometries having the same parameter (i.e k^+_{max} or ES, for instance), give rise to very different values of Roughness Function, confirming the achieved results of some recent literature findings (i.e. Kuwata and Nagura (2020)). Among the analyzed parameters, the Effective Slope has the better correlation, and the data are more or less aligned following a logarithmic law. This result is in agreement with the observations of Napoli et al. (2008). Even though a logarithmic relationship is visible (a law was recently suggested by De Marchis (2016)), a level of scatter can be found. Indeed, geometries having the same ES have differences in the ΔU^+ estimation of about 30%. In Fig. 5, and hereafter, the dotted lines represent the interpolating line, whereas the depicted gray region indicate the dispersion area of the achieved data. This deviation was quantified in term of Roughness Function, through a parameter indicated with ΔU_d^+. A discussion about this deviation is given in the following.

The correlations shown in Fig. 5a–e can be considered only partial adequate to predict the effect of rough walls on the mean flow, due to their scatter from the interpolating lines. On the other hand, looking at Fig. 5f, where ΔU^+ vs. k_s is depicted, an almost perfect correlation is found. Unfortunately, as previously mentioned, the equivalent sand grain roughness is not a geometrical parameter a-priori known. To assess the goodness of a specific combination, we can look at how well the interpolating line fits the numerical results. In order to this, the *Roughness Function dispersion* ΔU_d^+, was calculated. Specifically, it is obtained through the shift of the interpolating line either above and below the extreme data points. By measuring, in vertical direction, the distance between these extreme lines, a measure of the overall "scattering" can be obtained. A smaller ΔU_d^+ value indicates good correlation between the Roughness Function and the geometrical parameter, conversely a larger ΔU_d^+ suggests a less optimal combination. Looking at the Fig. 5a–e a significant dispersion of data points can be observed, leading to a high value of ΔU_d^+. On the other hand, the correlation with the equivalent sand grain roughness k_s^+, reported in Fig. 5f, is fine enough to have $\Delta U_d^+ = 2.0$, the smallest one.

In order to further investigate on the link between the corrugation shape and the energy dissipation, here other new geometrical parameters have been considered based on the roughness area A^{*+} (see Eqs. (6)–(9)). These parameters, reported in Table 3, are the area of peaks above the zero plane A_P^+; the peaks area above the absolute average deviation $A^+_{P\bar{k}}$; the area of the absolute value of Gaussian peaks and cavities $\overline{A}^+$; the area of the absolute value of Gaussian peaks and cavities above the absolute average deviation $\overline{A}^+_{\bar{k}}$. In Fig. 6 the dependence between the areal parameter A^{*+} and ΔU^+ is plotted. The figure illustrates a general augmentation of the Roughness Function with the corrugation area. Unfortunately, cannot be found a collapse of the data along a specific curve, as obtained for k_s^+. Focusing the attention on the single roughness group, for instance $I64$, all the data are aligned and follow a logarithmic law. The same rule applies for the other rough walls groups. Despite of this, the results are translated each other, and geometries having the same area generate huge difference in the downward shift estimations. This behavior is also demonstrated by the quantification of ΔU_d^+, with values spanning in the range between 5.19 and 7.14. The achieved results confirm how neither the areal parameters, neither the classical roughness statistics are able to predict the velocity reduction in the outer-layer. Basically, as already observed in the previous section, a single geometrical parameter is not able to characterize the wall roughness.

In order to find a correlation with ΔU^+, a combination of two parameters was analyzed. Some recent literature findings (see among others De Marchis et al., 2020; Jouybari et al., 2021), in fact, observed how the combination of two parameters, characteristic of the roughness density and distribution, can be the key to predict ΔU^+. In the following, the product between ES and a surface feature k^* is investigated. The choice to kept fixed ES and varies k^* is given by the good correlation of ES with ΔU^+ (plotted in Fig. 5e) and by the ability of ES to represent the roughness density. Specifically, the following joints are considered: $ES \cdot \overline{k}^+$, $ES \cdot \overline{k}^+_{max}$, $ES \cdot \overline{k}^+_{pv}$, $ES \cdot \overline{k}^+_{rms}$. The results, depicted in Fig. 7, clearly illustrate how the use of the roughness slope and a parameter representative of the roughness height reduces the scatter of the results. This can be also quantified through the low values of ΔU_d^+. Comparing Figs. 5b and 7b, where ΔU^+ vs $\overline{k}^+_{max}$ and ΔU^+ vs. $ES \cdot \overline{k}^+_{max}$ are plotted respectively, it can be argue how, taking into account both ES and $\overline{k}^+_{max}$, the data tend to collapse over a log-line and the ΔU_d^+ goes from 4.31 to 2.45, a value quite similar to that achieved for k_s^+. Similar results are observed for the other combinations reported. The findings are in agreement with the previous studies of De Marchis et al. (2020). Despite of this, the collapse shown in Fig. 7 is far from the alignment observed in Fig. 5f, where ΔU^+ vs. k_s^+ was reported, confirming the need to further investigate on the use of a couple of parameters.

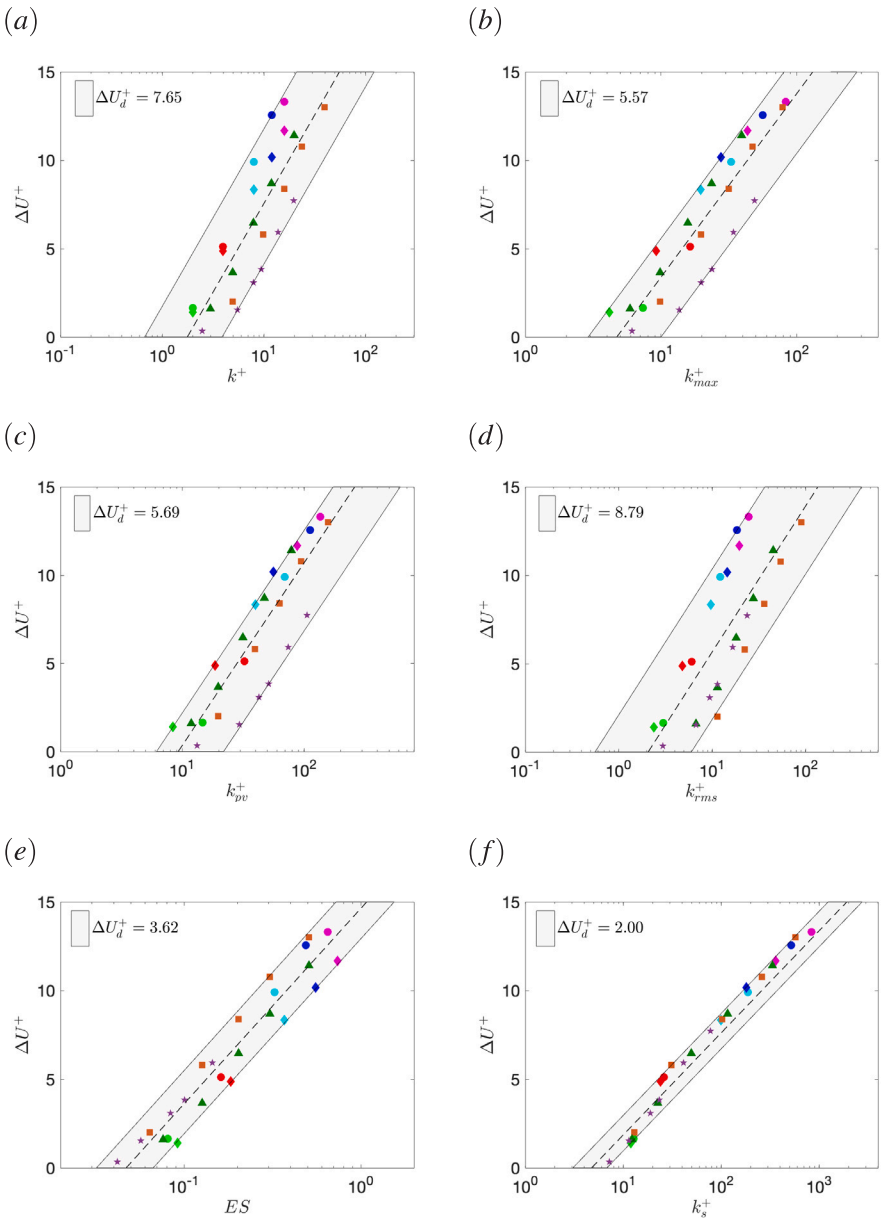

Fig. 5. Dependence of the Roughness Function ΔU^+ on geometrical parameters. (a) k^+: mean absolute deviation; (b) k^+_{max}: maximum roughness peak; (c) k^+_{pv}: maximum roughness peak-to-valley; (d) k^+_{rms} : root mean square of the roughness height; (e) ES: Effective Slope; (f) k^+_s: equivalent sand grain roughness.

Interestingly, when the product between the Effective Slope and a specific areal feature A^* is taken into account, an almost collapse of the data is achieved. The findings are plotted in Fig. 8, where the dependence of the Roughness Function on $ES{\cdot}A^+_P$, $ES{\cdot}A^+_{P\overline{k}}$, $ES{\cdot}\overline{A}^+$ and $ES \cdot \overline{A_{\overline{k}}}^+$ is reported. The good correlation can be explained considering that the slope is representative of the roughness steepness, whereas the proposed areal parameters are representative of the corrugation distribution, i.e. the amount of region occupied by solid roughness. Thanks to both parameters can be thus taken into account for the global feature of the roughness.

All cases are characterized by a visible alignment, where increasing the value of the geometrical parameter the Roughness Function raises. Nevertheless, among the four correlations, those related with the Area filtered by the absolute deviation $\overline{k}$ ($ES{\cdot}A^+_{P\overline{k}}$ and $ES{\cdot}\overline{A_{\overline{k}}}^+$), plotted in the left panels of Fig. 8, seem to be characterized by an highest collapse of the data along a straight line, in the semi-log plot. It is worthwhile to point out how the proposed correlation took into account the existing literature data of De Marchis et al. (2010) and De Marchis (2016), who investigate different roughness shapes, specifically 2D regular triangular roughness and irregular sinusoidal shapes. A good alignment is observed also for these geometries, suggesting the goodness of the

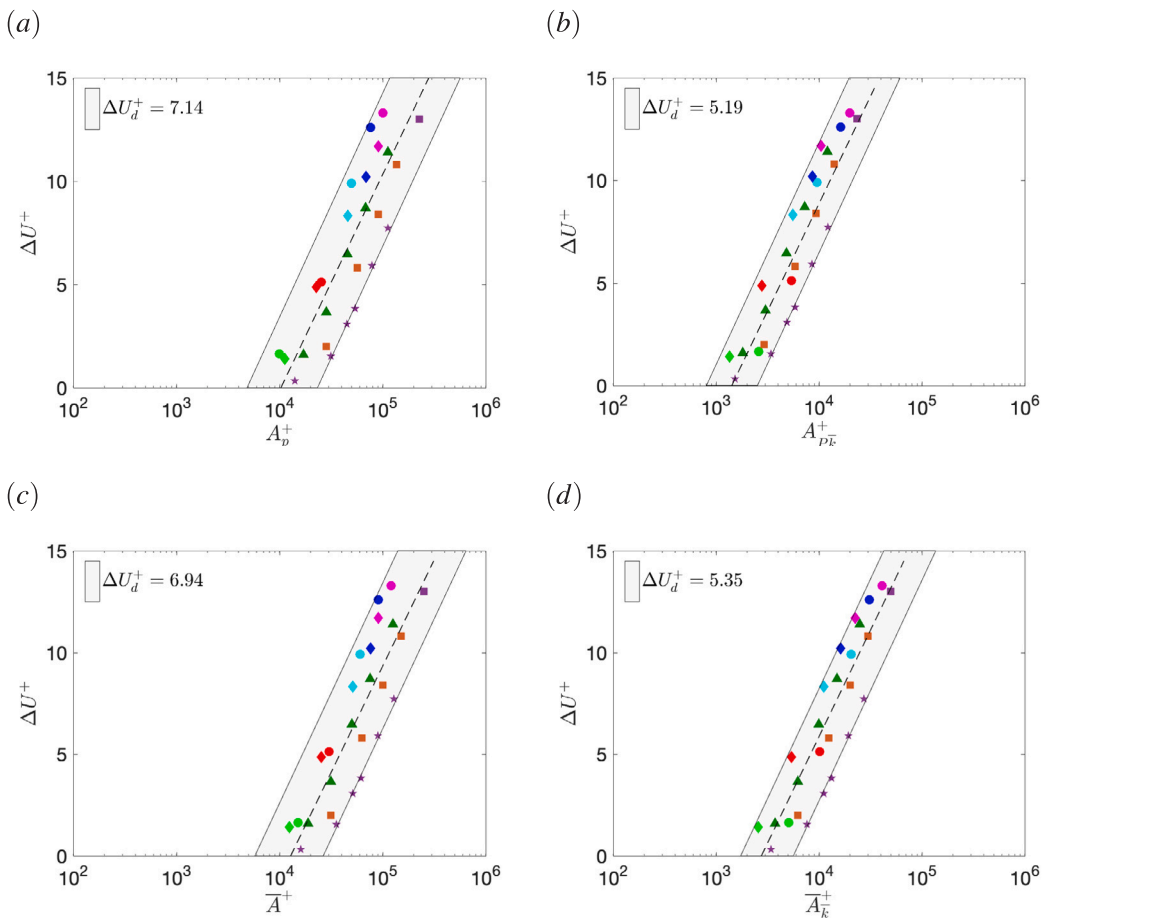

Fig. 6. Dependence of the Roughness Function ΔU^+ on the areal parameters. (a) A_P^+: Peaks area above the zero plane. (b) $A_{P\bar{k}}^+$: Peaks area above the absolute average deviation. (c) $\overline{A}^+$: Area of the absolute value of Gaussian peaks and cavities. (d) $\overline{A_{\bar{k}}}^+$: Area of the absolute value of Gaussian peaks and cavities above the absolute average deviation. The Area values are normalized with respect to friction Reynolds number and the kinematic viscosity, thus to achieve quantity in inner units.

proposed correlation. Following the pioneering work of Hama (1954), and the subsequent researches (see among others De Marchis et al., 2020; Ganju et al., 2022), in the figure the black line is given by the equation:

$$\Delta U^+ = \frac{1}{\kappa} ln(EA^*) + B + C \tag{13}$$

where B is the typical log law constant for smooth wall equal to 5.0, whereas C is a constant specific for each correlation. To improve the clarity, below the values of C achieved for each specific A^{*+} are reported: C = −21 for $ES \cdot A_P^+$; C = −16 for $ES \cdot A_{P\bar{k}}^+$; C = −21 for $ES \cdot \overline{A}^+$ and finally C = −18 for $ES \cdot \overline{A_{\bar{k}}}^+$. The coefficient C has been obtained thus to achieve the best fit of the numerical data. This best fit was obtained through the minimization of the least-square. According to the literature findings, the von Kàrmàn constant is equal to $\frac{1}{\kappa} = 0.4 \pm 0.02$. In addition, the method of regression analysis allowed to calculate the root-mean square error (RMSE) of all correlations investigated. Specifically, the following values were obtained, RMSE = 0.932 for ΔU^+ versus $ES \cdot A_P^+$, RMSE = 0.564 for ΔU^+ versus $ES \cdot A_{P\bar{k}}^+$, RMSE = 0.871 for ΔU^+ versus $ES \cdot \overline{A}^+$ and finally RMSE = 0.609 for ΔU^+ versus $ES \cdot \overline{A_{\bar{k}}}^+$. The same error calculation was applied also for the k_s^+, shown in Fig. 5f, which leaded to a value of RMSE = 0.445. The achieved results clearly show a very similar RMSE values obtained with k_s^+ and $ES \cdot A_{P\bar{k}}^+$, suggesting the ability of the proposed parameter to predict the downward shift of the mean velocity profiles. The above discussed results confirm how Roughness Function does not show consistent dependence on the single geometric parameter being considered (such as k^+, k_rms, k_pv or Es), whereas the combination of two parameters improve the Roughness Function estimation. In particular, the combination between ES and A^* allows to reduce the dispersion. Consequently the ΔU_d^+ value is very small compared to the previous cases. ΔU_d^+ achieve its lowest value, equal to 2.23, using $ES \cdot A_{P\bar{k}}^+$. This value is quite similar to that obtained for k_s^+, confirming the ability to have a reliable and accurate correlation. The parameter based on the Effective Slope ES and $A_{P\bar{k}}^+$ is defined as Effective Area EA and can be calculated according to the equation:

$$EA = \sum_{i=1}^{L_{x_1}} \left| \frac{dk(x_1)}{dx_1} \right| \cdot \sum_{i=1}^{32 \cdot jj} \beta \sum_{j=1}^{8/jj} \frac{1}{\sigma_i \sqrt{2\pi}} e^{-\frac{1}{2}\left(\frac{x_1(j)-\mu}{\sigma_i}\right)^2} \cdot dx_1 \tag{14}$$

The above analysis puts in light the possibility to estimate the Roughness Function once the roughness area is known. As previously stated, the Effective Area EA can be easily calculated through a scan surface of the physical domain of investigation. It can found direct application

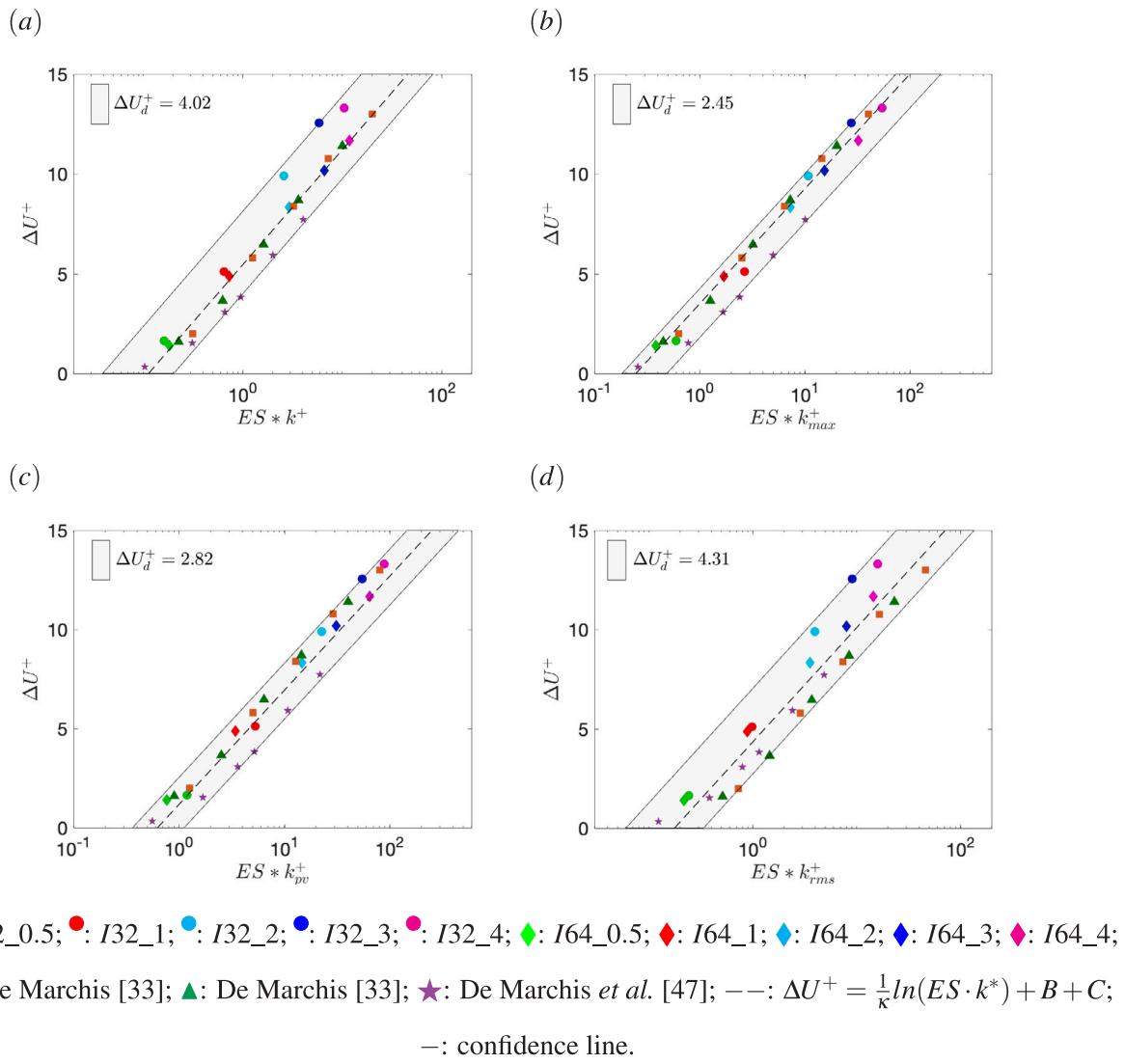

Fig. 7. Dependence of the Roughness Function ΔU^+ on geometrical parameters. (a) $ES \cdot k^+$; (b) $ES \cdot k^+_{max}$; (c) $ES \cdot k^+_{pv}$; (d) $ES \cdot k^+_{rms}$.

in engineering (i.e. roughness pipes or blade turbines degradation) as well as in environmental cases (i.e. land roughness or ripples). The above results were achieved over 2D rough shapes and clearly further simulations are required to confirm the proposed findings, including 3D regular and irregular rough geometries.

6. Conclusions

Large Eddy Simulations were carried out over irregular rough walls at friction Reynolds number $Re_\tau = 400$ in order to investigate on the downward shift of the streamwise mean velocity profile, known in literature as Roughness Function ΔU^+. A total of 10 simulations were performed over 2D rough surfaces designed throughout Gaussian function, having different average height of the oscillations, different distribution and different density. Specifically, turbulent channel flows were investigated at five increasing roughness average height equal to $\overline{k} = 0.005 \cdot h$, $\overline{k} = 0.01 \cdot h$, $\overline{k} = 0.02 \cdot h$, $\overline{k} = 0.03 \cdot h$ and $\overline{k} = 0.04 \cdot h$. For each value of roughness height, different roughness densities were considered and, specifically, two groups of roughness have been generated through the imposition of 32 or 64 subsequent positive and negative irregular Gaussian function. In order to investigate on the effect of roughness density and distribution, the mean velocity profiles were analyzed keeping constant the $\overline{k}$. The study clearly illustrate how, for small value of the mean roughness height, the profiles collapse each other (cases $I32\_0.5$ and $I64\_0.5$). Therefore, the roughness density and distribution do not affect the velocity reduction in the logarithmic region. The results, is also confirmed by the mean velocity profiles over rough walls having $\overline{k} = 0.01 \cdot h$. The mean velocity profiles obtained over geometries having $\overline{k} = 0.02 \cdot h$, clearly show how the energy dissipation is influenced by the roughness density. Basically, the lower the roughness density (32 Gaussian curves), the higher the downward shift of the velocity.

The mean velocity profile reduction was correlated to some geometrical parameters such as the equivalent sand grain roughness k_s^+, the mean roughness height $\overline{k}^+$, the peak-to-valley roughness height k_{pv}^+, the root mean square roughness height k_{rms}^+, the Effective Slope ES. The analysis pointed out that the velocity reduction in the streamwise direction is given by a combination of geometrical parameters and a single feature of the corrugation geometry may not be representative of the whole effect. In order to further investigate on the link between the corrugation shape and the energy dissipation, here other new geometrical parameters have been considered based on the roughness Area A^{*+}: the peaks area above the zero plane A_P, the peaks area above the absolute average deviation $A^+_{P\overline{k}}$, the area of absolute value of Gaussian peaks and cavities $\overline{A}^+$, the area of absolute value of Gaussian

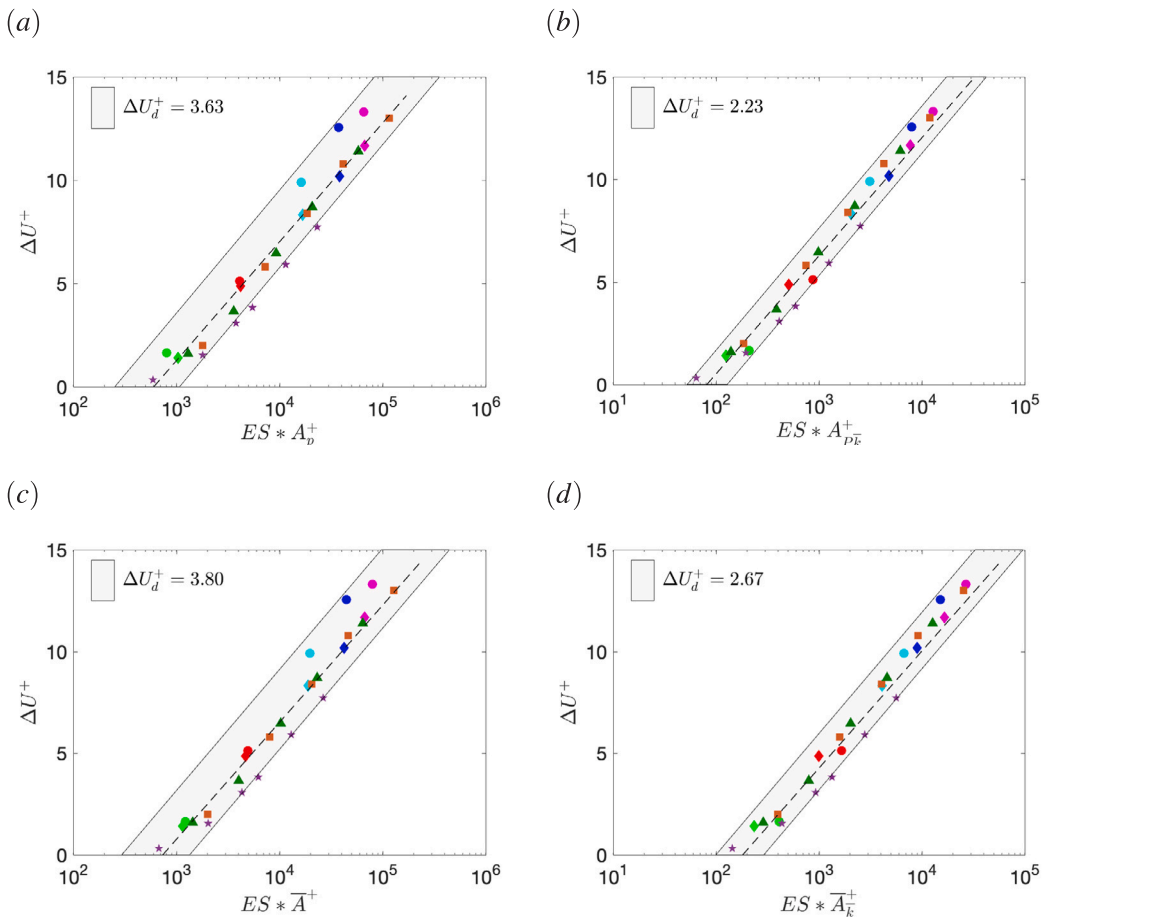

Fig. 8. Dependence of the Roughness Function ΔU^+ on the areal parameters. (a) $ES \cdot A_P^+$; (b) $ES \cdot A_{P\overline{k}}^+$; (c) $ES \cdot \overline{A}^+$; (d) $ES \cdot \overline{A}_{\overline{k}}^+$.

peaks and cavities above the absolute average deviation $\overline{A}_{\overline{k}}^*$. Looking at the dependence between the areal parameter A^{*+} and ΔU^+, it was not found a collapse of the data along a specific curve, as obtained for k_s^+. A combination of two parameters was, thus, analyzed, among others: $ES \cdot \overline{k}^+$, $ES \cdot k_{max}^+$, $ES \cdot k_{pv}^+$, $ES \cdot k_{rms}^+$, $ES \cdot A_P^+$, $ES \cdot \overline{A}_{P\overline{k}}$, $ES \cdot \overline{A}^+$, $ES \cdot \overline{A}_{\overline{k}}^+$. Comparing the correlation between ΔU^+ vs. k_{max}^+ and ΔU^+ vs. $ES \cdot k_{max}^+$, it was observed how taking into account both ES and k_{max}^+, the data collapsed over a line. Similar results was obtained for the other combinations $ES \cdot k^*$ investigated. Despite of this, the collapse was still far from the alignment achieved with ΔU^+ vs. k_s^+. On the other hand, when the product between the Effective Slope and a specific areal feature A^* was taken into account, an almost collapse of the data was observed. Therefore, results revealed how a single geometric parameter, whether ES or Area A, is insufficient to predict the roughness effect. Conversely, the combination of these two parameters improves predictive accuracy, at least for the proposed roughness model. This improvement can be attributed to ES ability to interpret the roughness distribution and height and to A^{*+} ability to take into account for the coverage area over a flat plate. The major goal of this study was the introduction of the new geometrical parameter defined as the Effective Area EA, based on the combination between the Effective Slope ES and the peaks Area above the absolute average deviation $A_{P\overline{k}}^+$. A good correlation between the ΔU^+ and EA was achieved, at least for 2D Gaussian roughness. Further investigations are required to confirm the proposed law in a wider range of 3D roughness configurations. The numerical simulations here performed suggest that the Effective Area EA is able to predict ΔU^+, similarly to the equivalent sand grain roughness k_s.

CRediT authorship contribution statement

F. Bruno: Writing – original draft, Writing – review & editing. **M. De Marchis:** Writing – original draft, Writing – review & editing. **E. Napoli:** Writing – original draft, Writing – review & editing.

Declaration of competing interest

The authors declare that they have no known competing financial interests or personal relationships that could have appeared to influence the work reported in this paper.

Data availability

Data will be made available on request.

Acknowledgments

The authors greatly appreciate the financial support provided by the following projects:

- RETURN Extended Partnership and received funding from the European Union Next-GenerationEU (National Recovery and Resilience Plan – NRRP, Mission 4, Component 2, Investment 1.3 – D.D. 1243 2/8/2022, E0000005);
- TiSento - SENSORIALIZED COMPOSITE PIPE FOR HYDRAULIC APPLICATIONS, n. 084221000550 CUP G18I18001710007. Funded under measure 1.1.5 of the PO FESR SICILY 2014–2020;
- SiciliAn MicronanOTecH Research And Innovation CEnter "SAMOTHRACE" (MUR, PNRR-M4C2, ECS-00000022), spoke 3 - Università degli Studi di Enna "S2-COMMs - Micro and Nanotechnologies for Smart & Sustainable Communities".

References

Abdelaziz, M., Djenidi, L., Ghayesh, M.H., Chin, R., 2022. A new equivalent sand grain roughness relation for two-dimensional rough wall turbulent boundary layers. J. Fluid Mech. 940, A25.

Anderson, W., Barros, J.M., Christensen, K.T., Awasthi, A., 2015. Numerical and experimental study of mechanisms responsible for turbulent secondary flows in boundary layer flows over spanwise heterogeneous roughness. J. Fluid Mech. 768, 316–347. http://dx.doi.org/10.1017/jfm.2015.91.

Antonia, R.A., Krogstad, P.-A., 2001. Turbulence structure in boundary layers over diierent types of surface roughness. Fluid Dyn. Res. 28, 139–157.

Ashrafian, A., Andersson, H.I., Manhart, M., 2004. DNS of turbulent flow in a rod-roughened channel. Int. J. Heat Fluid Flow 25, 373–383. http://dx.doi.org/10.1016/j.ijheatfluidflow.2004.02.004.

Barros, J.M., Schultz, M.P., Flack, K.A., 2018. Measurements of skin-friction of systematically generated surface roughness. Int. J. Heat Fluid Flow 72, 1–7.

Bhaganagar, K., Kim, J., Coleman, G., 2004. Effect of roughness on wall-bounded turbulence. Flow Turbul. Combust. 72, 463–492. http://dx.doi.org/10.1023/B:APPL.0000044407.34121.64.

Bons, J., 2005. A critical assessment of Reynolds analogy for turbine flows. J. Heat Transfer 127, 472–485. http://dx.doi.org/10.1115/1.1861919.

Busse, A., Lützner, M., Sandham, N.D., 2015. Direct numerical simulation of turbulent flow over a rough surface based on a surface scan. Comput. & Fluids 116, 129–147. http://dx.doi.org/10.1016/j.compfluid.2015.04.008.

Busse, A., Thakkar, M., Sandham, N.D., 2017. Reynolds-number dependence of the near-wall flow over irregular rough surfaces. J. Fluid Mech. 810, 196–224. http://dx.doi.org/10.1017/jfm.2016.680.

Chan, L., Macdonald, M., Chung, D., Hutchins, N., Ooi, A., 2015. A systematic investigation of roughness height and wavelength in turbulent pipe flow in the transitionally rough regime.

Chung, D., Hutchins, N., Schultz, M.P., Flack, K.A., 2021. Predicting the drag of rough surfaces. Annu. Rev. Fluid Mech. 53, 439–471. http://dx.doi.org/10.1146/annurev-fluid-062520-115127.

De Marchis, M., 2016. Large eddy simulations of roughened channel flows: Estimation of the energy losses using the slope of the roughness. Comput. & Fluids 140, 148–157. http://dx.doi.org/10.1016/j.compfluid.2016.09.021.

De Marchis, M., Milici, B., Napoli, E., 2019. Large eddy simulations on the effect of the irregular roughness shape on turbulent channel flows. Int. J. Heat Fluid Flow 80, http://dx.doi.org/10.1016/j.ijheatfluidflow.2019.108494.

De Marchis, M., Napoli, E., 2012. Effects of irregular two-dimensional and three-dimensional surface roughness in turbulent channel flows. Int. J. Heat Fluid Flow 36, 7–17. http://dx.doi.org/10.1016/j.ijheatfluidflow.2012.04.003.

De Marchis, M., Napoli, E., Armenio, V., 2010. Turbulence structures over irregular rough surfaces. J. Turbul. 11, 1–32. http://dx.doi.org/10.1080/14685241003657270.

De Marchis, M., Saccone, D., Milici, B., Napoli, E., 2020. Large eddy simulations of rough turbulent channel flows bounded by irregular roughness: Advances toward a universal roughness correlation. Flow Turbul. Combust. 105, 627–648. http://dx.doi.org/10.1007/s10494-020-00167-5.

Flack, K.A., Schultz, M.P., 2010. Review of hydraulic roughness scales in the fully rough regime. J. Fluids Eng. Trans. ASME 132, 0412031–04120310. http://dx.doi.org/10.1115/1.4001492.

Flack, K.A., Schultz, M.P., 2014. Roughness effects on wall-bounded turbulent flows. Phys. Fluids 26, http://dx.doi.org/10.1063/1.4896280.

Flack, K.A., Schultz, M.P., Volino, R.J., 2020. The effect of a systematic change in surface roughness skewness on turbulence and drag. Int. J. Heat Fluid Flow 85, http://dx.doi.org/10.1016/j.ijheatfluidflow.2020.108669.

Forooghi, P., Stroh, A., Magagnato, F., Jakirlić, S., Frohnapfel, B., 2017. Toward a universal roughness correlation. J. Fluids Eng. Trans. ASME 139, http://dx.doi.org/10.1115/1.4037280.

Ganju, S., Bailey, S.C., Brehm, C., 2022. Amplitude and wavelength scaling of sinusoidal roughness effects in turbulent channel flow at fixed $\{\{Re\}_\tau = 720\}$. J. Fluid Mech. 937, http://dx.doi.org/10.1017/jfm.2022.118.

Garg, H., Wang, L., Sahut, G., Fureby, C., 2023. Large eddy simulations of fully developed turbulent flows over additively manufactured rough surfaces. Phys. Fluids 35 (4).

Hama, F.R., 1954. Boundary layer characteristics for smooth and rough surfaces.

Jouybari, M.A., Yuan, J., Brereton, G.J., Murillo, M.S., 2021. Data-driven prediction of the equivalent sand-grain height in rough-wall turbulent flows. J. Fluid Mech. 912, http://dx.doi.org/10.1017/jfm.2020.1085.

Kuwata, Y., Kawaguchi, Y., 2019. Direct numerical simulation of turbulence over systematically varied irregular rough surfaces. J. Fluid Mech. 862, 781–815.

Kuwata, Y., Nagura, R., 2020. Direct numerical simulation on the effects of surface slope and skewness on rough-wall turbulence. Phys. Fluids 32, http://dx.doi.org/10.1063/5.0024038.

Lee, S., Yang, J., Forooghi, P., Stroh, A., Bagheri, S., 2022. Predicting drag on rough surfaces by transfer learning of empirical correlations. J. Fluid Mech. 933, http://dx.doi.org/10.1017/jfm.2021.1041.

Leonardi, S., Castro, I.P., 2010. Channel flow over large cube roughness: A direct numerical simulation study. J. Fluid Mech. 651, 519–539. http://dx.doi.org/10.1017/S002211200999423X.

Leonardi, S., Orlandi, P., Smalley, R.J., Djenidi, L., Antonia, R.A., 2003. Direct numerical simulations of turbulent channel flow with transverse square bars on one wall. J. Fluid Mech. 491, 229–238. http://dx.doi.org/10.1017/S0022112003005500.

Ligrani, P.M., Moffat, R.J., 1986. Structure of transitionally rough and fully rough turbulent boundary layers. J. Fluid Mech. 162, 69–98.

Maaß, C., Schumann, U., 1996. Direct numerical simulation of separated turbulent flow over a wavy boundary. Flow Simulation with High-Performance Computers II: DFG Priority Research Programme Results 1993–1995. Springer, pp. 227–241.

Macdonald, M., Chan, L., Chung, D., Hutchins, N., Ooi, A., 2016. Turbulent flow over transitionally rough surfaces with varying roughness densities. J. Fluid Mech. 804, 130–161. http://dx.doi.org/10.1017/jfm.2016.459.

Mejia-Alvarez, R., Christensen, K.T., 2013. Wall-parallel stereo particle-image velocimetry measurements in the roughness sublayer of turbulent flow overlying highly irregular roughness. Phys. Fluids 25, http://dx.doi.org/10.1063/1.4832377.

Milici, B., De Marchis, M., 2016. Statistics of inertial particle deviation from fluid particle trajectories in horizontal rough wall turbulent channel flow. Int. J. Heat Fluid Flow 60, 1–11. http://dx.doi.org/10.1016/j.ijheatfluidflow.2016.03.008.

Moody, L.F., 1944. Friction factors for pipe flow. Trans. Asme 66, 671–684.

Moser, R.D., Kim, J., Mansour, N.N., 1999. Direct numerical simulation of turbulent channel flow up to Re τ= 590. Phys. Fluids 11 (4), 943–945.

Napoli, E., Armenio, V., De Marchis, M., 2008. The effect of the slope of irregularly distributed roughness elements on turbulent wall-bounded flows. J. Fluid Mech. 613, 385–394. http://dx.doi.org/10.1017/S0022112008003571.

Nikuradse, J., 1993. Laws of flow in rough pipes.

Nugroho, S., Nugroho, B., Fusil, E., Chin, R., 2023. Effects of varied roughness coverage area on drag in a turbulent boundary layer using numerical simulations. Ocean Eng. 287, 115721.

Orlandi, P., Leonardi, S., Antonia, R.A., 2006. Turbulent channel flow with either transverse or longitudinal roughness elements on one wall. J. Fluid Mech. 561, 279–305. http://dx.doi.org/10.1017/S0022112006000723.

Sarakinos, S., Busse, A., 2022. Investigation of rough-wall turbulence over barnacle roughness with increasing solidity using direct numerical simulations. Phys. Rev. Fluids 7 (6), 064602.

Schlichting, H., 1937. Experimental Investigation of the Problem of Surface Roughness, vol. 823, National Advisory Commitee for Aeronautics.

Schultz, M.P., Flack, K.A., 2009. Turbulent boundary layers on a systematically varied rough wall. Phys. Fluids 21, http://dx.doi.org/10.1063/1.3059630.

Sigal, A., Danberg, J.E., 1990. New correlation of roughness density effect on the turbulent boundary layer. AIAA J. 28, 554–556. http://dx.doi.org/10.2514/3.10427.

Thakkar, M., Busse, A., Sandham, N., 2017. Surface correlations of hydrodynamic drag for transitionally rough engineering surfaces. J. Turbul. 18, 138–169. http://dx.doi.org/10.1080/14685248.2016.1258119.

Van Rij, J.A., Belnap, B.J., Ligrani, P.M., 2002. Analysis and experiments on three-dimensional, irregular surface roughness. J. Fluids Eng. Trans. ASME 124, 671–677. http://dx.doi.org/10.1115/1.1486222.

Waigh, D.R., Kind, R.J., 1998. Improved aerodynamic characterization of regular three-dimensional roughness. AIAA J. 36, 1117–1119. http://dx.doi.org/10.2514/2.491.

Yang, Y., Wu, G., Ren, K., 2022. Hydroelastic wave diffraction by a vertical circular cylinder standing in a channel with an ice cover. J. Fluid Mech. 941, A13. http://dx.doi.org/10.1017/jfm.2022.284.

Yuan, J., Piomelli, U., 2014. Estimation and prediction of the roughness function on realistic surfaces. J. Turbul. 15, 350–365. http://dx.doi.org/10.1080/14685248.2014.907904.

Zang, Y., Street, R.L., Koseff, J.R., 1993. A dynamic mixed subgrid-scale model and its application to turbulent recirculating flows. Phys. Fluids A: Fluid Dyn. 5 (12), 3186–3196.

Zhen Ma, G., Xu, C.X., Sung, H.J., Huang, W.X., 2022. Scaling of rough-wall turbulence in a transitionally rough regime. Phys. Fluids 34, http://dx.doi.org/10.1063/5.0084646.